Noname manuscript No.
(will be inserted by the editor)

Analysis and Design of Trajectory-Based Operations under Wind Forecast Uncertainty

Dun Yuan Tan · Sandeep Badrinath · Hamsa Balakrishnan

Received: date / Accepted: date

Abstract The Trajectory-Based Operations (TBO) concept is a key part of the FAA's and EUROCONTROL's programs to make flight operations more efficient and predictable, while maintaining operational flexibility. TBO relies on four dimensional (4D) trajectories that are managed by specifying a sequence of metering points. Each metering point is associated with a controlled time of arrival (CTA) that must be met by the aircraft within a specified time tolerance. Although the TBO concept has been around for a while, prior literature has not addressed design aspects, such as identifying metering point locations and their impact on the system performance.

In this paper, we show how a prior analytical model for TBO can be adapted to account for wind forecast uncertainty, and other operational constraints. We investigate the influence of different system parameters such as wind forecast uncertainty, distance between metering points, and CTA tolerance. The analysis reveals interesting trade-offs between various performance metrics such as throughput, fuel burn and delay. Based on this analysis, we propose a framework for locating metering points to satisfy traffic demand, while being fuel efficient.

Keywords Trajectory-Based Operations · Wind Forecast Uncertainty · Performance analysis · Air traffic management

1 Introduction

The Trajectory-Based Operations (TBO) concept represents a paradigm shift in air traffic management from the traditional clearance-based control to trajectory-based

D. Y. Tan · S. Badrinath · H. Balakrishnan
Department of Aeronautics and Astronautics
Massachusetts Institute of Technology
Cambridge, MA, USA
E-mail: {tandun, sandeepb, hamsa}@mit.edu

This work was supported in part by the FAA (under award number 80895-Z9411201) and NASA (under grant number 80NSSC19K1607).

control by utilizing 4-Dimensional Trajectories (4DTs) and system-wide sharing of information as the basis for flight planning and execution [1]. The TBO concept is an integral part of FAA's NextGen as well as EUROCONTROL's SESAR programs, and is planned to be operational during this coming decade. By managing flights based on their position in time (time-based flow management), TBO will provide a predictable and accurate trajectory [2]. TBO also promises optimized trajectories and the capability to fly optimal routes using Performance-Based Navigation (PBN), leading to higher efficiency and throughput, and lower delays and fuel burn. With higher automation under the TBO concept, the responsibility of the air traffic controllers will shift from managing individual aircraft to managing air traffic streams/flows, resulting in lower controller workload and the ability to manage higher traffic densities.

The 4D description of a trajectory within the TBO concept includes a set of 3D metering points from the departure gate to the arrival gate. Each metering point is associated with a controlled time of arrival (CTA) that must be met by the aircraft within a specified time tolerance [3]. Aircraft can use the Required Time of Arrival (RTA) functionality in their Flight Management Systems (FMS) to meet the CTAs. There have been several field trials of the TBO concept, including demonstrations of the RTA functionality of an aircraft to meet a metering point at a desired CTA [4,5]. The field trials at KSEA performed by the FAA using the B737 indicated that the aircraft can meet the specified CTA with high accuracy [4]. However, many operational issues such as pilot/controller workload, information sharing, and time-horizon of the CTA operation were identified [4,6].

1.1 Existing work

Researchers have analyzed issues related to the time-horizon of the CTA operation and the desired tolerance using analytical models and simulations [7,8]. Simulation-based studies incorporating the aircraft dynamics have been used to determine the probability of not meeting the CTA, and the probability of loss of separation [9, 8]. Analytical models have been proposed to compute the trajectory uncertainty and queuing delays while reaching a metering point [7,10]. In particular, De Smedt et al. [7] proposed a model based on a differential equation in order to represent the trajectory deviation under wind forecast uncertainty. This model could estimate the required speed corrections for CTA operation, and the time-horizon within which an aircraft could reliably reach a metering point within the desired tolerance.

In addition to the trajectory deviation and CTA tolerance, an important factor that impacts the system performance is the location of metering points. A multi-stage model proposed by Chen and Solak [11] selects the number and position of metering points during optimized profile descent. There have also been studies that have focused on determining an optimal control law to reach a metering point at the desired CTA, accounting for system uncertainties [12,13]. However, most of the prior work has focused on a single metering point in the terminal arrival airspace, even though the TBO concept calls for a gate-to-gate trajectory with a sequence of metering points.

1.2 Contributions of this paper

Although the vision for TBO has been well established, there are several unanwsered questions regarding the optimal architecture to support TBO and to establish operational requirements for the system. In particular, there are challenges surrounding the selection and placement of metering points, as well as the required tolerance at these metering points, in the presence of uncertainty. This paper therefore aims to answer the following questions:

- What are the key system parameters associated with CTA operations in a TBO environment?
- What are the trade-offs between the various design parameters, and what is their impact on metrics such as throughput, fuel burn and delay?
- How should the optimal number and location of metering points be determined?

To answer these questions, we develop a mathematical model for the trajectory uncertainty by extending a prior model [7]. The new model accounts for more realistic operations such as maximum speed correction constraint and FMS wind blending. We then present a parametric analysis of the relationship between the various system parameters, and use this information to identify optimal locations of metering points along a route.

2 Model for Trajectory Uncertainty

A model for the longitudinal uncertainty in aircraft's position is presented to understand the trade-offs between the system parameters. In a TBO environment, an aircraft follows a sequence of metering points, meeting each point at a specified controlled time of arrival (CTA). Such an operation can be carried out in practice by entering the required CTA as a constraint in the aircraft's flight management system (FMS). However, the actual wind speed might deviate from the forecast wind speed, resulting in a deviation from the planned or predicted trajectory. The FMS needs to use the necessary speed correction to meet the required CTA at the metering point. We therefore develop a model for trajectory deviation under wind forecast uncertainty with speed corrections from the FMS.

We first present a model for the deviation from the flight's predicted trajectory considering just a single metering point, and later use those results to extend it to the case when there is a sequence of metering points. We assume that the aircraft is following a one dimensional trajectory (representing the cruise phase of flight) and adapt a model that was presented by De Smedt et al. [7]. We account for additional constraints that are more representative of the actual operations, such as allowable speed correction and FMS wind blending.

Let x_{act} and x_{pred} denote the actual and predicted trajectory, respectively. Note that the predicted trajectory is the planned trajectory based on the wind forecasts. The along-track longitudinal uncertainty in the predicted trajectory (x) is given by:

$$x = x_{act} - x_{pred} \tag{1}$$

The predicted trajectory is based on a nominal ground speed (V_{pred}), and is computed using the following dynamics:

$$\frac{dx_{pred}}{dt} = V_{pred}(t) \tag{2}$$

Let $w(t)$ be the wind forecast uncertainty, defined as the difference between the realized wind (W_a) and the forecast wind (W), that is, $w(t) = W_a(t) - W(t)$. A positive value for $w(t)$ indicates either that the tailwind is underestimated, or that the headwind is overestimated. Let $s(t)$ be the speed correction by the FMS to correct for the longitudinal deviation from the predicted trajectory. Then, the dynamics of the actual trajectory in the presence of the wind forecast uncertainty is given by:

$$\frac{dx_{act}}{dt} = V_{pred}(t) + w(t) - s(t) \tag{3}$$

The dynamics for the longitudinal uncertainty can be obtained using Eqs. (1- 3):

$$\frac{dx}{dt} = w(t) - s(t) \tag{4}$$

Consider a scenario wherein the next metering fix needs to be reached at $t = CTA$ within a particular tolerance for the final deviation ($|x_f| \leq x_{tol}$). Note that a tolerance specified using distance can be translated into a tolerance in time using the nominal speed. Such a specification can be achieved by using a speed correction strategy that is given by [7]:

$$s(t) = \begin{cases} \frac{x(t)}{CTA-t}, & t \leq t_1 \\ s(t_1), & t > t_1 \end{cases}; \quad t_1 = CTA - \frac{x_{tol}}{w_0} \tag{5}$$

This specification assumes that the wind forecast uncertainty is bounded by some maximum wind uncertainty (i.e., $w(t) = w_0$). An intuitive interpretation of the presented policy is that the amount of speed correction depends on the longitudinal deviation ($x(t)$), and the correction needs to be higher when one is closer to the metering fix in order to achieve the desired tolerance (i.e, there is a dependence on $(CTA - t)$). Additionally, there exists a particular time t_1 that depends on the desired tolerance and maximum wind uncertainty (w_0), beyond which, a constant speed correction of $s(t_1)$ is sufficient to ensure that the aircraft is within the desired tolerance at CTA. More details on the derivation of the control strategy and validation using a FMS simulation can be found in the original paper [7]. Integrating Eq. (4) using the speed correction policy (Eq. (5)), one obtains the following expression for the longitudinal uncertainty:

$$x(t) = \begin{cases} x_0 \frac{CTA-t}{CTA-t_0} - w_0(CTA-t)\ln\left(\frac{CTA-t}{CTA-t_0}\right), & t \leq t_1 \\ x_{tol} + x_0 \frac{CTA-t}{CTA-t_0} - w_0(CTA-t)\left[1 - \ln(\frac{w_0(CTA-x_{tol})}{x_{tol}})\right], & t > t_1 \end{cases} \tag{6}$$

Here, x_0 represents the longitudinal trajectory deviation at the initial time, t_0. Illustration of the model parameters along with a typical profile for longitudinal deviation and speed correction is shown in Fig. 1. Operationally, such a speed correction profile

makes sense because one wants to have a very small control effort initially to hedge against the fact that the wind disturbances cancel out. The corresponding longitudinal deviation shows that the deviation increases to reach a maximum and then decreases to be within the desired tolerance. Using the expressions for the longitudinal deviation and speed correction, we can obtain the maximum possible deviation (x_{max}):

$$x_{max} = \max\{\exp\left(-1+\frac{x_0}{w_0(CTA-t_0)}\right) w_0(CTA-t_0), x_f\} \tag{7}$$

Here, x_f represents the final deviation at the CTA, which is equal to x_{tol} in this case. Fig. 1 illustrates the case in which the wind forecast uncertainty is positive, and hence a positive speed correction is required to slow down the aircraft to reach the metering point. On the other hand, when the wind forecast uncertainty is negative, the speed correction ($s(t)$) needs to be negative to speed up the aircraft.

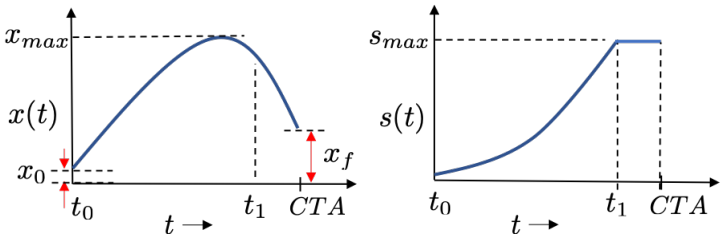

(a) Longitudinal deviation ($x(t)$) (b) Speed correction ($s(t)$)

Fig. 1: Illustration of the model parameters ($|x_f| \leq x_{tol}$ is desired).

2.1 Incorporating the maximum speed correction constraint

The speed correction strategy in Eq. (5) assumes that there is no constraints on the maximum or minimum speeds of the aircraft. Therefore, we present a modification to the earlier model to include a constraint on the allowable speed correction. We assume that the aircraft can perform a speed correction up to a negotiated maximum value of $\hat{s}_{max}$. This constraint on the maximum speed correction might however result in the aircraft not meeting the desired tolerance at the CTA.

Let s'_{max} denote the required maximum speed correction to meet a desired tolerance. The maximum speed correction possible can be smaller or larger than the required value. If the maximum feasible speed correction is larger than the required value, then the earlier analysis without any constraints holds true, and the aircraft is within the desired tolerance at the CTA. When the maximum speed correction is smaller than the required value ($s'_{max} \leq \hat{s}_{max}$), the speed correction policy needs to be saturated at $\hat{s}_{max}$:

$$s(t) = \begin{cases} \frac{x(t)}{CTA-t}, & t \leq \hat{t}_1 \\ \hat{s}_{max}, & t > \hat{t}_1 \end{cases} \tag{8}$$

where $\hat{t}_1 = CTA - (CTA - t_0)\exp\left(\frac{1}{w_0}(\frac{x_0}{CTA-t_0} - \hat{s}_{max})\right)$. Here, $\hat{t}_1$ is the time instant when the required speed correction given by Eq. (5) equals $\hat{s}_{max}$, and can be obtained by substituting Eq. (6) in Eq. (8). In general, when the maximum feasible speed correction is smaller or larger than the required value, the following holds true with regards to the realized maximum speed correction (s_{max}) and the time when the speed correction saturates (t_1):

$$(s_{max}, t_1) = \begin{cases} (s'_{max}, t'_1) & s'_{max} \leqslant \hat{s}_{max} \\ (\hat{s}_{max}, \hat{t}_1), & s'_{max} \geqslant \hat{s}_{max} \end{cases} \tag{9}$$

Here, t'_1 indicates the time when the speed correction saturates for the case in which there are no speed constraints, as given by Eq. (5). Substituting for the speed correction policy in the dynamics, one obtains the longitudinal deviation profile for the general case:

$$x(t) = \begin{cases} x_0\frac{CTA-t}{CTA-t_0} - w_0(CTA-t)\ln\left(\frac{CTA-t}{CTA-t_0}\right), & t \leqslant t_1 \\ w_0(t-t_1) + s_{max}(CTA-t), & t \geqslant t_1 \end{cases} \tag{10}$$

The final deviation ($x_f = x(CTA)$) can be computed using Eqs. (9) and (10):

$$x_f = \begin{cases} x_{tol}, & s'_{max} \leqslant \hat{s}_{max} \\ w_0(CTA-t_0)\exp(\frac{1}{w_0}(\frac{x0}{CTA-t_0} - \hat{s}_{max})), & s'_{max} \geqslant \hat{s}_{max} \end{cases} \tag{11}$$

Note that the final deviation equals to the desired tolerance when the negotiated speed correction constraint is larger than the required maximum speed correction. However, when the former condition is not true, the final deviation depends on many factors and has implications on the growth or decay of trajectory uncertainty in the case of a sequence of metering points (further discussed in Section 5). The expression for maximum deviation (x_{max}) will be the same as given in Eq. (7).

2.2 Impact of FMS wind blending

The analysis presented earlier did not account for FMS wind blending. In actual operations, the FMS blends the wind profile using a combination of the forecast and sensed winds, to yield a lower wind uncertainty [14]. The resulting FMS wind is equal to the sensed wind in the near field, the forecast in the far field, and a weighted average of the forecast and sensed winds in between. Assuming that the nominal trajectory and the wind forecast are updated at every metering point before starting the CTA operation for the next metering point, the wind uncertainty at the start ($t = t_0$) is equal to zero because it is based on sensed winds, and the wind uncertainty at $t = CTA$ is based on just the forecast (i.e, w_0). Based on linear interpolation, we consider the following time-varying wind uncertainty profile for the blended-wind forecast:

$$w(t) = \frac{w_0}{CTA}t \tag{12}$$

The model for time-varying wind uncertainty in Eq. (12) can also be interpreted as increasing wind forecast uncertainty with a lookahead time [15]. We can substitute

the blended-wind uncertainty profile in the dynamics for the longitudinal deviation, and use the speed correction policy to obtain expressions for the longitudinal deviation as done earlier in Section 2.1. We obtain the following expression for the case without any constraints on the speed correction.

$$x(t) = \begin{cases} x_0 \frac{CTA-t}{CTA-t_0} - w_0(CTA-t)\left[\ln\left(\frac{CTA-t}{CTA-t_0}\right) + \frac{t-t_0}{CTA}\right], & t \leqslant t_1 \\ \frac{w_0(t^2-CTA^2)}{2CTA} + \frac{CTA-t}{CTA-t_1'}x(t_1') + x_{tol}, & t \geqslant t_1 \end{cases} \tag{13}$$

$$t_1 = \sqrt{CTA(CTA - 2\frac{xtol}{w_0})} \tag{14}$$

We have skipped the mathematical details for the sake of brevity. Similar expressions can be obtained when there is a constraint on the maximum speed correction. Illustration of the trajectory profiles with and without wind blending are shown in Fig. 2. We can observe a reduction in the longitudinal uncertainty and the required speed correction with wind-blending.

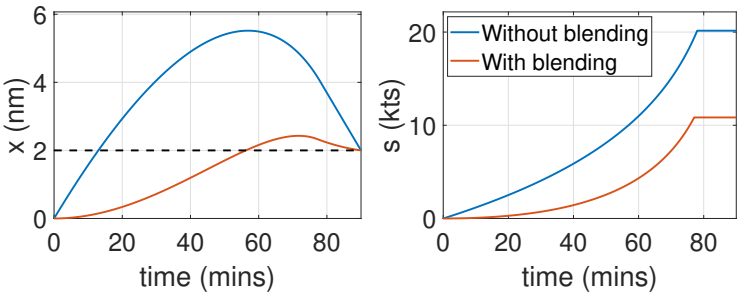

(a) Longitudinal uncertainty (b) Speed correction

Fig. 2: Trajectory profiles with and without wind blending (CTA = 120 min, $x_{tol} = 2$ NM, $x_0 = 0$ NM, $w_0 = 10$ kts).

3 Performance Metrics

We consider three metrics of the system performance, namely throughput, delay and fuel burn.

3.1 Throughput

We define link throughput, H_{link}, as the number of aircraft that can pass through a link (connecting two metering points) per unit time. The link throughput is given by $H_{link} = 1/t_{sep}$, where t_{sep} denotes the required separation time between two aircraft. The separation time is given by the required separation distance between two aircraft divided by the aircraft ground speed. To compute the required separation distance,

one needs to consider the maximum longitudinal uncertainty that can be there on any link (x_{max}) in addition to the minimum ATC specified separation (x_{req}). This is because aircraft separation is guaranteed by assigning appropriate CTAs at the metering points, accounting for position uncertainty. A conservative estimate for the required minimum separation is therefore $2x_{max}+x_{req}$ (a factor of two is used because we need to consider position uncertainty of both the leader and follower aircraft). Additionally, we assume that all aircraft along a flow corridor are constrained to fly at the same nominal speed. The realized ground speed with speed correction and wind uncertainty is given by, $V_{GS}(t) = V_{pred} + w(t) - s(t)$. The throughput of the link is constrained by the minimum ground speed on the link because of speed correction, $V_{GS,min} = V_{pred} + w_0 - s_{max}$. Therefore, the link throughput is given by:

$$H_{link} = \frac{1}{t_{sep}} = \frac{V_{pred} + w_0 - s_{max}}{2x_{max} + x_{req}}. \tag{15}$$

3.2 Delay

We define delay as the difference between the actual arrival time at a metering fix and the required CTA. We compute the delay based on the aircraft's deviation at the metering point (x_f) and its ground speed. The deviation of the aircraft's trajectory from its planned trajectory at the CTA signifies the additional distance it has traveled (if x_f is positive), or the additional distance it needs to travel in order to meet the metering point (if x_f is negative). A positive x_f represents the aircraft being ahead of the metering point at CTA. This corresponds to the aircraft passing the metering point before the assigned CTA in our framework. Therefore, to align our definition of delay to the convention that a positive delay signifies arriving late, we include a negative sign for x_f in our definition for delay:

$$delay = \frac{-x_f}{V_{GS}(CTA)}. \tag{16}$$

3.3 Fuel burn

The fuel burn is evaluated using BADA model 3.0. The nominal fuel flow rate (f_{nom}) for the cruise phase of flight is calculated using thrust (T) and the true airspeed (V_{TAS}):

$$f_{nom}(t) = C_{f1}\left(1 + \frac{V_{TAS}(t)}{C_{f2}}\right)T(t). \tag{17}$$

Here, C_{f1} and C_{f2} are aircraft specific coefficients from the BADA model. The aircraft thrust (T) in cruise phase at constant altitude is given by

$$T(t) = D(t) + m(t)\frac{dV_{TAS}}{dt}, \tag{18}$$

where, m denotes aircraft mass. The true airspeed, $V_{TAS}(t) = V_{GS}(t) - W_a(t)$, where W_a is the actual wind speed. We define the wind forecast uploaded onto the flight plan

as $W(t)$, so the actual wind, $W_a(t) = W(t) - w(t)$. For the fuel burn computation, we assume zero forecast windspeed, primarily to have the wind uncertainty ($w(t)$) as the key dependent parameter in our analysis. Therefore, $V_{TAS}(t) = V_{GS}(t) - w(t) = V_{pred} + 2w(t) - s(t)$. The drag term in Eq. (18) is obtained using the following standard expressions:

$$D(t) = \frac{1}{2} C_D(t) \rho V_{TAS}(t)^2 S; \tag{19}$$

$$C_D(t) = C_{D_0} + \alpha C_L(t)^2; \quad C_L(t) = \frac{m(t)g}{\frac{1}{2}\rho V_{TAS}(t)^2 S} \tag{20}$$

Here, C_{D_0} and α are drag polar coefficients. The thrust and fuel flow rate along a trajectory are computed by discretizing Eq. (18) and accounting for the decrease in aircraft mass, $m(t+1) = m(t) - \frac{f(t)}{\Delta t}$. The average fuel flow rate (f_{avg}) and total fuel flow rate (F_{tot}) for CTA operations are given by:

$$f_{avg} = \frac{1}{CTA - t_0} \int_{t_0}^{CTA} f_{nom}(t) dt; \quad F_{tot} = \int_{t_0}^{CTA} f_{nom}(t) dt \tag{21}$$

We use model coefficients for A320 for the analysis presented in this paper. Note that a similar analysis can be obtained for other aircraft types, but the general trends remain the same.

4 Parametric Analysis of Tradeoffs

In this section, we analyze the tradeoffs between the system parameters and performance metrics. A parametric analysis is performed to understand the impact of the various system parameters (CTA, x_0, x_{tol}, w_0, and $\hat{s}_{max}$) with the two trajectory uncertainty models (with and without wind blending). The parametric analysis is performed by varying a particular parameter of interest and fixing other parameters at a nominal value. We first present the parametric analysis of two key variables in detail: CTA (that equivalently represents the distance between metering points) and w_0 (weather forecast uncertainty). The impact of other parameters are summarized later in Section 5.

4.1 Impact of distance between metering points

The CTA represents the time at which the aircraft needs to be at the next metering point starting from the current metering point. We investigate the impact of the distance between metering points through a parametric analysis of the CTA. For the parametric analysis, the CTA is varied from 20 mins to 180 mins, which translates to a distance of 166 NM to 1,500 NM between the metering points (considering a constant nominal ground speed of 500 kts). We fix the values of other parameters in the model: $x_0 = 0$ NM, $x_{tol} = 1$ NM, $w_0 = 10$ kts, $t_0 = 0$ and $\hat{s}_{max} = 25$ kts.

Fig. 3(a) shows the contour plots for trajectory deviation and speed correction profile with different CTAs for the case without wind blending. We notice that for a

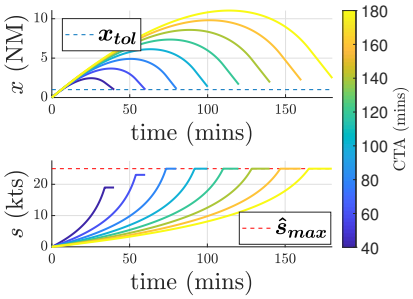

(a) Profile of $x(t)$ and $s(t)$ without blending

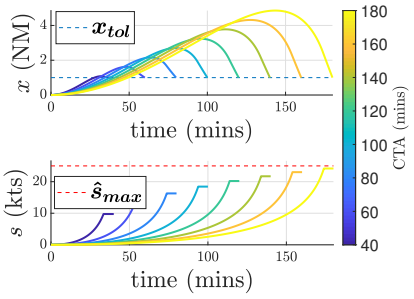

(b) Profile of $x(t)$ and $s(t)$ with blending

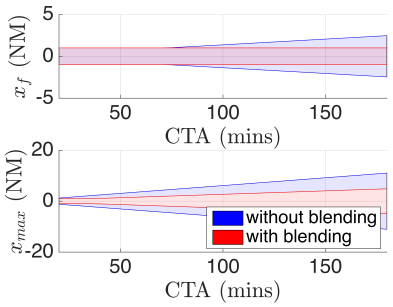

(c) x_f and x_{max} for varying CTA

Fig. 3: Parametric analysis with varying CTA ($x_0 = 0\ NM$, $x_{tol} = 1\ NM$, $w_0 = 10\ kts$ and $\hat{s}_{max} = 25\ kts$.)

shorter CTA (closer to the metering point), the maximum possible deviation (x_{max}) is lower and requires a lower maximum speed correction (s_{max}). However, for $CTA \geq 75$ mins, the maximum speed correction required to meet the tolerance at the meeting point (s'_{max}) is greater than the maximum allowable speed correction ($\hat{s}_{max}$) and therefore, the final deviation (x_f) is greater than the desired tolerance. A similar trend is observed for the case with wind blending (Fig. 3(b)). However, the required maximum speed correction is lower than the speed constraint ($\hat{s}_{max}$) because of lower wind forecast uncertainty as a result of blending, yielding the desired final tolerance at the metering fix.

Fig. 3(c) shows the bounds for x_{max} and x_f for various CTAs. The bounds were obtained by considering positive and negative values of the wind forecast uncertainty ($\pm w_0$) in the trajectory deviation profile (Eq. (10)). The shaded area in the figure represents the range of maximum deviation and final deviation because of wind forecast uncertainty. We notice that the maximum trajectory deviation is smaller with wind blending. Additionally, we observe that for CTA greater than 75 min, the final deviation at the fix is greater than the tolerance for the case without blending. It should be noted that the final deviation at the fix can exceed the desired tolerance even with wind blending for a larger wind forecast uncertainty. Therefore, the system parameters (CTA, x_{tol}) need to be appropriately chosen while considering constraints on

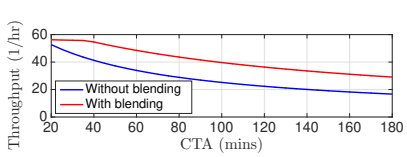

(a) Throughput (1/hr)

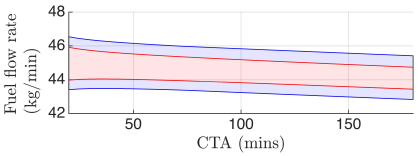

(b) Average fuel flow rate (kg/min)

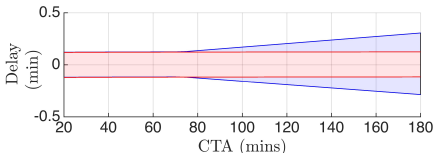

(c) Delay (min)

Fig. 4: Influence of CTA on performance metrics(with and without wind blending).

$(w_0, \hat{s}_{max})$ such that the aircraft is capable of meeting the desired tolerance, while ensuring a lower delay so that there will not be a significant impact on subsequent links. Additionally, a higher speed correction is required for a better CTA accuracy.

Fig. 4 illustrates the influence of varying CTA on the different performance metrics. The variation of link throughput for different CTAs is shown in Fig. 4(a). We see that throughput decreases with increase in CTA due to the increase in maximum longitudinal deviation (x_{max}). Therefore, link throughput reduces with an increase in distance between metering points. However, reducing the distance between the metering points to improve the throughput would result in a larger number of metering points along the route, which could lead to higher controller workload. Finally, the throughput is higher with wind blending because of lower maximum deviation.

The average fuel flow rate, which is also indicative of the control effort, decreases with increase in CTA as shown in Fig. 4(b) (the bounds in the figure are obtained by considering $\pm w_0$). One can intuitively understand such a trend by imagining an extreme case in which the metering points are so closely spaced that the aircraft follows a precise 4D trajectory, which would require very high control effort. This yields an interesting trade-off: with an increase in CTA (distance between metering points), the fuel flow rate decreases; however, the throughput also decreases. Therefore, the distance between the metering points needs to be appropriately chosen such that the throughput satisfies the traffic demand while being fuel efficient.

Figure 4(c) illustrates the variation of the delay window with CTA. The delay window is obtained from the final deviation, x_f, in Fig. 3(c). The region where delay window remains constant represents the feasible CTA for which the final deviation is within the desired tolerance. However, when the final deviation exceeds the tolerance, x_{tol}, the delay window increases with wind forecast uncertainty, as seen in Fig. 4(c).

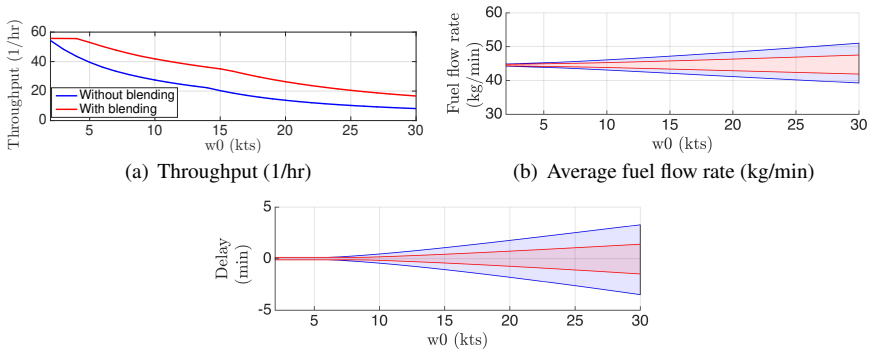

(a) Throughput (1/hr)

(b) Average fuel flow rate (kg/min)

(c) Delay (min)

Fig. 5: Performance metrics for varying w_0 (with and without wind blending).

4.2 Impact of wind forecast uncertainty

We investigate the impact of different levels of wind forecast uncertainty (w_0) on operations through a parametric analysis by varying w_0 and fixing other parameter values: $x_0 = 0$ NM, $x_{tol} = 1$ NM, $CTA = 90$ mins, $t_0 = 0$ and $\hat{s}_{max} = 25$ kts. In general, for low values of w_0, the maximum required speed correction is smaller than the permissible limit ($\hat{s}_{max}$), and hence the final deviation is equal to the desired tolerance. However, beyond a threshold value for the wind forecast uncertainty, the final deviation can exceed the desired tolerance. This threshold point is higher with wind blending than without wind blending.

Figure 5 shows the variation of the performance metrics for different levels of wind forecast uncertainty. The throughput decreases with increase in wind forecast uncertainty as expected because of higher longitudinal uncertainty. The variability in the fuel flow rate increases with wind forecast uncertainty (Fig. 5(b)), while the average fuel flow rate remains almost constant with increasing wind forecast uncertainty because the positive and negative components of wind uncertainty cancel each other out. Moreover, the delay window increases with increase in wind uncertainty because of higher final deviation. The above analysis quantifies the improvement in system performance (delay, fuel burn, throughput) with better wind forecasts, and can inform investments toward improving weather forecast accuracy.

4.3 Feasible Solution space

We determine the feasible parameter space of (CTA, x_0, s_{max}) that can achieve a desired tolerance at the metering point for a given wind forecast uncertainty. Figure 6 summarizes the parametric analyses with contours indicating the throughput and average fuel flow rate. The shaded region in Fig. 6 also represents the feasible parameter space over which the combination of system parameters can achieve the desired tolerance at the metering point. In addition to the feasible space, these plots reveal the trade-off between the throughput and fuel burn. The decision-maker can

use such plots for selecting the metering points (CTA) along a route to accommodate the demand while optimizing fuel burn.

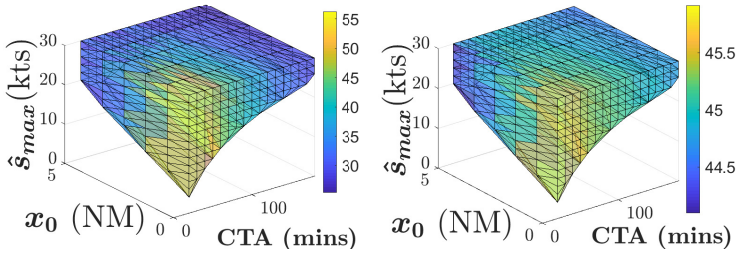

(a) Throughput contours (1/hr) (b) Fuel flow rate contours (kg/min)

Fig. 6: Feasible parameter space with wind blending

5 Implications to system design

The results from the parametric analysis are summarized in Table 1, corresponding to the case when the trajectory is capable of meeting the desired final tolerance. The delay window in the table represents the on-time uncertainty (the maximum difference between the earliest and latest arrival time) at the metering point. Note that the delay window will not change for a given value of desired tolerance. The key insights from the analysis are the following:

- A larger distance between metering points (higher CTA) requires a smaller number of metering points along the route. This results in a lower controller effort in terms of managing a smaller number of metering points, as well as lower aircraft fuel burn. However, the downside is that the link throughput decreases and one needs to have a lower density of air traffic along that route.
- Higher wind forecast uncertainty results in lower throughput and higher fuel burn. Our results quantified the marginal improvement in throughput and fuel efficiency with better wind forecasts. This analysis can be used as a key input for driving investment decisions for better wind forecasts. Additionally, for a higher weather forecast uncertainty, aircraft need to execute a higher speed correction that may be infeasible.
- Higher accuracy at the metering point (lower tolerance) leads to a lower delay window. However, one may need to have a larger speed correction to achieve a higher accuracy, leading to higher fuel burn.

5.1 Metering Points in Sequence

We utilize the results and insights for a single link to analyze the performance when we have a sequence of metering points along a route. In this case, the final deviation (x_f) at a metering point becomes the initial deviation (x_0) for the CTA operation at the

Table 1 Summary of parametric analysis

Parameter	Throughput	Mean average fuel burn rate	Bounds for fuel flow rate	Delay window
Higher CTA	(↓)	(↓)	(↔)	(↔)
Higher w_0	(↓)	(↑)	(↑)	(↔)
Higher x_0	(↓)	(↓)	(↓)	(↔)
Higher x_{tol}	(↑)	(↓)	(↑)	(↑)

Notation: increases (↑), decreases (↓), constant (↔)

subsequent metering point. The exponential term in the expression for x_f (Eq. (11)) dictates whether the final deviation across subsequent metering points will grow or decay. Based on Eq. (11), the final deviation across subsequent links (with the same CTA) will grow exponentially if the following condition is satisfied:

$$\frac{x_0}{CTA - t_0} - \hat{s}_{max} \geqslant 0 \implies (CTA - t_0)\hat{s}_{max} \leqslant x_0 \tag{22}$$

Here, $(CTA - t_0)\hat{s}_{max}$ represents the maximum distance that can be corrected using the speed correction. If the maximum distance that can be corrected for exceeds the initial deviation, then the deviation would grow. If the negotiated speed correction constraint ($\hat{s}_{max}$) is capable of meeting the tolerance at the metering fix (x_{tol}), then the tolerance at the previous metering fix determines the maximum initial deviation possible at the current link (x_0). Therefore, it is important to appropriately choose the location of metering points and the desired tolerance such that the negotiated tolerance at subsequent metering fixes can be satisfied, while minimizing for total fuel burn. Additionally, a lower tolerance should be specified at metering points in the terminal airspace or where merging occurs to have higher certainty (smaller delay window) and increased throughput. The link throughput (H_{link}) also plays an important role in scheduling CTAs for flights along a route. The flights along the same route must be scheduled such that the separation time at the metering point, which is specified by assigning appropriate CTAs, must be at least equal to the required safe separation time, $t_{sep} = 1/H_{link}$ (based on Eq. (15)).

6 Design problem: Optimally locating metering points

The results of the parametric analysis can be used to optimize the locations of metering points. For particular values of wind forecast uncertainty, desired CTA tolerance, and maximum speed correction value, we determine empirical relationships for the throughput and fuel flow rate as a function of CTA. Using these relationships, we develop an optimization framework to select metering points from among N candidate waypoints, so as to minimize total fuel burn while satisfying the demand for throughput along the route.

6.1 Throughput and Fuel Flow Rate as Functions of the CTA

The empirical relationships of the throughput and fuel flow rate as functions of CTA for a particular set of the system parameters ($w_0 = 15$ kts, $\hat{s}_{max} = 30$ kts, $x_{sep} = 5$ NM, $x_0 = x_{tol} = 1$ NM) are shown in Fig. 7. The initial deviation is chosen to be equal to the desired final tolerance, as we are considering a sequence of metering points.

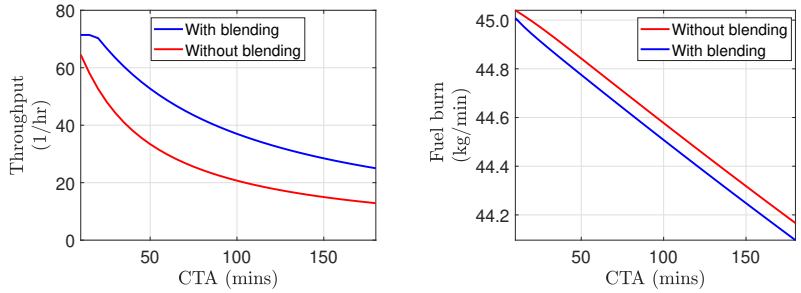

(a) Throughput vs CTA (b) Average fuel flow rate vs CTA

Fig. 7: Performance metrics as a function of CTA (surrogate for the distance between metering points)

We observe in Fig. 7 that the relationship between the throughput and CTA is almost quadratic for the region where the trajectory deviation is not constrained by the desired tolerance (i.e. for CTA $>$ 20 min), and that the relationship between the average fuel flow rate and the CTA is almost linear. We therefore obtain expressions for throughput and fuel burn as functions of CTA for given wind forecast uncertainty, initial deviation, tolerance, and maximum speed correction as follows:

$$H_{link} = \alpha_{th}\,\mathrm{CTA}^2 + \beta_{th}\mathrm{CTA} + \gamma_{th} \tag{23}$$

$$f_{i,j} = \alpha_f\,\mathrm{CTA} + \beta_f. \tag{24}$$

The parameters α_{th}, β_{th}, γ_{th} are constants obtained by fitting a quadratic curve to the maximum throughput. Similarly, α_f and β_f are obtained through a linear curve fit of the mean fuel flow rate. The coefficients for the case with FMS wind blending are given below (the R-squared values are both over 0.99, indicating a good fit):

$$[\alpha_{th}, \beta_{th}, \gamma_{th}] = [0.0018, -0.6108, 79.1127] \tag{25}$$

$$[\alpha_f, \beta_f] = [-0.0053, 45.0395] \tag{26}$$

6.2 Optimization Framework for Choosing Metering Points

6.2.1 Notation

The notation used in the model formulation is as follows (Fig. 8):

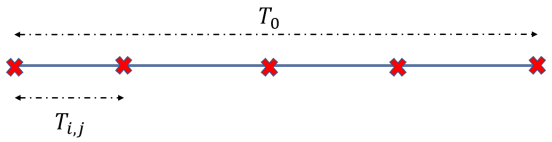

Fig. 8: Illustration of the notation used in the model formulation (crosses represent the waypoints along the route)

- $T_{i,j} \equiv$ Nominal flight time between waypoints i and j; $(i,j) \in 1,2....N$.
- $T_0 \equiv$ Total flight time for a given trajectory along a route.
- $x_{i,j} \equiv$ Binary decision variable that equals one if waypoints i and j are chosen as metering fixes, and waypoints between them are not chosen (i.e., there exists a link between i and j).
- $d_{i,j} \equiv$ Number of aircraft passing through a link connecting two waypoints (i,j) per unit time, representative of the demand.
- $H_{i,j} \equiv$ Throughput: number of aircraft that can safely pass through a link (i,j) per unit time.
- $f_{i,j} \equiv$ Average fuel flow rate per flight along the link connecting two metering points (i,j).

In our formulation, we define link demand, $D_{i,j}$, between any two metering points i and j as the maximum demand observed over all the sub-links between i and j (because any of the sub-links could be a bottleneck):

$$D_{i,j} = \max(d_{i,i+1}, d_{i+1,i+2}...d_{j-1,j}) \tag{27}$$

The functional relationships for the link throughput ($H_{i,j}$) and average fuel flow rate ($f_{i,j}$) are obtained using the parametric analysis (Eq. (23-24)). Note that one could transform the distance between waypoints into an equivalent time using nominal speeds planned along the route. Using Eq. (23-24), one obtains the following expressions for link throughput ($H_{i,j}$) and average fuel flow rate ($f_{i,j}$):

$$H_{i,j} = \alpha_{th}\, T_{i,j}^2 + \beta_{th} T_{i,j} + \gamma_{th} \tag{28}$$

$$f_{i,j} = \alpha_f\, T_{i,j} + \beta_f \tag{29}$$

6.2.2 Problem formulation

The optimal metering points along a route are obtained as a solution to the following integer program:

$$\min \quad \sum_{i=1}^{N}\sum_{j=1}^{N}\left[f_{i,j}x_{i,j}\times\left(\sum_{m=i}^{j-1}D_{m,m+1}T_{m,m+1}\right)\right] \tag{30a}$$

$$\text{s.t} \quad H_{i,j} \geq D_{i,j}x_{i,j} - M(1-x_{i,j}),\ \ \forall i,j \in N \tag{30b}$$

$$\sum_{i=1}^{N}\sum_{j=1}^{N} x_{i,j}\ T_{i,j} = T_0 \tag{30c}$$

$$\sum_{i=1}^{q-1} x_{i,q} = 1,\ \sum_{j=q+1}^{N} x_{q,j} = 1,\ \ \forall q \in Q \tag{30d}$$

$$\sum_{i=1}^{j-1} x_{i,j} \leq 1,\ \sum_{j=i+1}^{N} x_{i,j} \leq 1 \tag{30e}$$

$$\sum_{k=i}^{j-1}\sum_{\substack{m=i+1\\ m\neq j}}^{N} x_{k,m} + \sum_{k=1}^{i-1}\sum_{m=i+1,}^{j-1} x_{k,m} \leq N(1-x_{i,j}) \tag{30f}$$

$$x_{i,j} \leq 0,\ \text{for}\ j \leq i,\ \ i,j = 1,2...n \tag{30g}$$

$$x_{i,j} \in \{0,1\},\ i,j = 1,2...n \tag{30h}$$

Here, Q is a set of waypoints along the route that must necessarily be chosen as metering points (for example, waypoints at crossing flows), and M is an arbitrarily large number to enforce the constraint to be active when $x_{i,j}$ is zero.

The cost function is the the total fuel burn along the route, which is obtained by summing the product of flight demand, flight time, and fuel flow rate per unit time over the sub-links along the route. The cost is minimized with the following constraints:

1. The throughput for every link should be greater than the given demand for that link (30b).
2. Sum of the flight time over each of the links joining the metering points should be equal to total flight time, T_0 (30c).
3. Eq (30d) enforces that a pre-specified set of waypoints, Q, need to be strictly chosen as metering points (for example, this might be needed for managing crossing flows or merging flows).
4. For any waypoint i, there should be at most one outgoing link (30e).
5. For any link chosen between waypoints i and j, there should be no other smaller link chosen in between these two waypoints or a link intersecting these two waypoints, (30f).
6. The links are considered to be unidirectional to prevent double counting (30g), and (30h) represents non-negativity constraint.

We note that the solution to the above problem locates optimal metering points along a single route between two airports (for the level phase of flight). This method-

ology can be extended to all the routes in the airspace by solving the problem along individual routes. Additionally, a trajectory with multiple pre-specified metering points (representing constraint (30d)) can be further decomposed into smaller subproblems, further reducing the computational effort.

6.3 Illustrative example along a single route

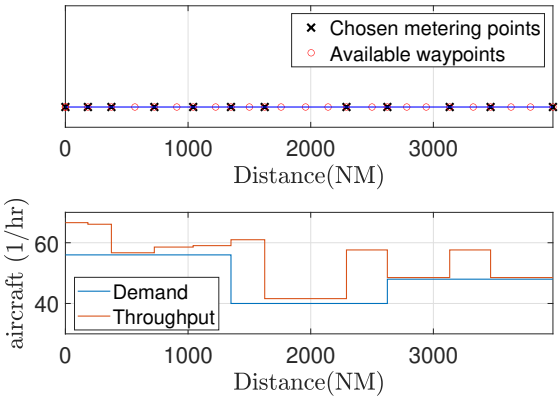

Fig. 9: Metering points chosen from a set of available fixes (top) to accommodate the varying demand (bottom).

In this section, we illustrate the solution to the optimal metering point selection using a simplified example. Consider a scenario where the length of the trajectory is 4000 NM with several waypoints or fixes along the route that are spaced at irregular intervals, as shown in Fig. 9. The demand (number of flights per hour) along the route includes demand arising from multiple OD segments and therefore can vary along the route, as shown in the bottom of Fig. 9. For illustration, we consider higher demands near the origin and the destination to represent higher traffic density near the terminal airspace. One is interested in identifying optimal metering points from a set of candidate fixes such that the throughput of each link (between the selected metering points) satisfies the underlying demand, and the route is fuel efficient. The required tolerance at all metering points is considered to be 1 NM for illustrative purposes.

To solve this problem using the presented framework, the distance along the trajectory is converted to an equivalent time using the planned speed profile along the route. The location of the optimal metering points obtained from the optimization are indicated using a cross in Fig. 9. The resulting link throughout along the trajectory is greater than the demand. Also, note that the throughput does not exactly match the demand because metering points are chosen from pre-existing fixes that are irregularly spaced. Additionally, one notices the higher density of metering points near the destination to accommodate higher demand and traffic density.

7 Discussions

7.1 Limitations of the analytical model

Although the analytical model presented in Section 2 enables closed-form analysis to yield promising results, it has certain limitations. The model assumes that all aircraft types on the same flow corridor have the same nominal speed. Additionally, it does not consider a mixed equipage environment, which can lead to different FMS having different speed correction policies. Moreover, the analytical speed correction policy does not explicitly depend on the wind forecast uncertainty or the maximum allowed speed correction (which could also vary with time).

7.2 Ongoing work

To address the key limitations of the analytical model, we are currently working on a robust optimization framework that can determine an optimal speed correction strategy with an objective to minimize fuel burn, while explicitly accounting for wind forecast uncertainty. The constraints include the desired tolerance at metering points as well as the maximum allowable speed correction which could be time varying. Additionally, one can consider uncertainty in off-block times and parameters associated with the speed correction policy to mimic different FMSs (arising from mixed equipage). The results from the robust optimization could be used to determine a less conservative relationship between the performance metrics and CTA. Additionally, we can extend our framework to determine optimal metering points in a network for the entire NAS.

8 Conclusions

We presented an analytical model for longitudinal deviation of an aircraft under wind forecast uncertainty in a TBO environment. We extended an earlier model [7] to account for initial deviation at a metering fix, maximum speed correction constraints and FMS wind blending. Our analysis revealed the influence of different system parameters (such as the distance between metering points, wind forecast uncertainty, and desired tolerance) on performance metrics such as throughput, delay and fuel burn. The following are the key takeaways: (a) Metering points should be closely spaced in high density airspace and, (b) nearer metering points results in higher throughput but also higher fuel burn. The analysis also quantified the marginal benefits of throughput and fuel efficiency through better wind forecasts, which could drive investment decisions regarding better weather forecasts. We also provided a framework to identify metering points along any trajectory, to satisfy the traffic demand along the route while being fuel efficient.

In addition to the cruise phase of flight that was the focus of this paper, one also needs to account for airport surface and terminal airspace operations in order to realize gate-to-gate TBO. Moreover, one could also incorporate current procedures

such as miles-in-trail restrictions, as well as more realistic spatial and temporal wind forecast uncertainty models [15] in the analysis.

References

1. FAA, "Concept of Operations for the Next Generation Air Transportation System, Version 3.2," https://apps.dtic.mil/dtic/tr/fulltext/u2/a535795.pdf, 2011, retrieved Oct 4, 2019.
2. FAA, "The Future of the NAS," https://www.faa.gov/nextgen/media/futureofthenas.pdf, 2016, retrieved Oct 4, 2019.
3. G. Enea and M. Porretta, "A comparison of 4D-trajectory operations envisioned for Nextgen and SESAR, some preliminary findings," in *28th Congress of the International Council of the aeronautical sciences*, 2012, pp. 23–28.
4. C. Wynnyk, M. Balakrishna, P. MacWilliams, and T. Becher, "2011 Trajectory Based Operations Flight Trials," *Proc. of 10th USA/Europe ATM R&D Seminar, Chicago, Illinois*, 2013.
5. L. H. Mutuel, E. Paricaud, and N. Pierre, "Initial 4D Trajectory Management Concept Evaluation," in *Proc. of 10th USA/Europe Air Traffic Management Research and Development Seminar*, 2013.
6. J. K. Klooster, A. Del Amo, and P. Manzi, "Controlled Time of Arrival Flight Trials – Results and Analysis," in *Proc. of 8th USA/Europe Air Traffic Management Research and Development Seminar*, 2009.
7. D. De Smedt, J. Bronsvoort, and G. McDonald, "Model for longitudinal uncertainty during controlled time of arrival operations," in *11th USA/Europe Air Traffic Management Research and Development Seminar*, 2015.
8. Á. Rodríguez-Sanz, C. C. Puchol, F. G. Comendador, J. Pérez-Castán, R. A. Valdés, F. S. Martínez, and M. N. Godoy, "Air traffic management based on 4D-trajectories: requirements and practical implementation," in *MATEC Web of Conferences*, vol. 304. EDP Sciences, 2019, p. 05001.
9. D. De Smedt and J. K. Klooster, "Controlled Time-of-Arrival Spacing Analysis," in *9th USA/Europe Air Traffic Management Research and Development Seminar*, 2011.
10. T. Nikoleris and M. Hansen, "Queueing models for trajectory-based aircraft operations," *Transportation Science*, vol. 46, no. 4, pp. 501–511, 2012.
11. H. Chen and S. Solak, "Optimal Metering Policies for Optimized Profile Descent Operations at Airports," in *Proc. of 6th International Conference on Research in Air Transportation, Istanbul, Turkey*, 2014.
12. S. Shresta, T. Gaydos, and W. Kirkman, "Evaluating intervention strategies for metering in the presence of trajectory uncertainty," in *Integrated Communications, Navigation and Surveillance Conference*, April 2012, pp. 1–23.
13. W. Kirkman, T. L. Gaydos, and L. A. Weitz, "Optimizing Metering for Trajectory Timing Uncertainty," in *AIAA Guidance, Navigation, and Control Conference*, 2014, p. 1462.
14. Honeywell, "Differentiating fms wind inputs and blending," https://aerospace.honeywell.com/en/learn/about-us/news/2019/06/differentiating-fms-wind-inputs-and-blending, 2019, retrieved Jan 24, 2020.
15. T. Reynolds, Y. Glina, S. Troxel, and M. McPartland, "Wind Information Requirements for NextGen Applications Phase 1: 4D-Trajectory Based Operations (4D-TBO)," *MIT Lincoln Laboratory*, 2013.